Impact of northward tropical cyclones on ozone in Southeastern China

Shanshan Ouyang[1,2], Tao Deng[2], Jingyang Chen[3], Run Liu[1,4], Xiaoyang Chen[2], Jinnan Yuan[2], Yanyan Huang[2], Shaw Chen Liu[1,4]

[1]College of Environment and Climate, Institute for Environmental and Climate Research, Jinan University, Guangzhou, 511443, China
[2]Guangdong Provincial Key Laboratory of Regional Numerical Weather Prediction, Guangzhou Institute of Tropical and Marine Meteorology of China Meteorological Administration, GBA Academy of Meteorological Research, Guangzhou, 510640, China
[3]Guangdong Ecological Meteorological Centre, Guangzhou 510640, China
[4]Guangdong-Hongkong-Macau Joint Laboratory of Collaborative Innovation for Environmental Quality, Jinan University, Guangzhou, 511443, China

Correspondence to: Tao Deng (tdeng@gd121.cn) and Shaw Chen Liu (shawliu@jnu.edu.cn)

Abstract. Ozone pollution in Southeastern China (SEC) during autumn are usually influenced by tropical cyclones (TCs). Based on statistical analysis, WRF-CMAQ simulation, and TC vortex filtering method, this study explores the effects of the intensity and location of northward TCs on ozone in SEC. Results show that the interannual fluctuations of autumn maximum daily 8 hour average ozone from 2014 to 2024 are mainly affected by northward TCs with intensities reaching typhoon (TY) or above level. As TCs intensify to TY, the photochemical activity, horizontal transport, and vertical mixing in SEC all develop to levels favorable for pollution, which jointly lead to higher ozone compared to other TC intensities. Although ozone remains high when TC intensity exceeds TY, further enhancement is inhibited by meteorological constraints, as evidenced by simulations of two severe ozone pollution episodes with intensifying TCs. In addition, comparing with the sensitivity experiment without TCs reveal that intense solar radiation combined with peripheral northerly winds during the northward TCs period elevated ozone by over 10 ppb, with changes in biogenic emissions contributing approximately 1~3 ppb. Moreover, when TCs are located near 20°N, they primarily enhance ozone through photochemical production and horizontal transport, with impacts on the southern SEC persisting even after TCs make landfall at 30°N. Finally, it is important to recognize the non-linear interaction between TCs and large-scale circulation such as the western Pacific subtropical high, which modulates TC tracks and intensity and subsequently influences ozone levels in the SEC and even across the eastern China.

1 Introduction

Tropospheric ozone (O_3) is a product of photochemical reaction between volatile organic compounds (VOCs) and nitrogen oxides (NOx) under sunlight (Lu et al., 2019). It is a typical secondary pollutant and one of the important factors causing the complex air pollution in China (Professional Committee of Ozone Pollution Control of Chinese Society for

Environmental Sciences, 2024; Trainer et al., 2000; Zhan et al., 2023). Excessive surface ozone concentration has adverse effects on both human health (Jacob and Winner, 2009) and ecosystems (Grulke and Heath, 2020). In addition to large-scale

35   anthropogenic emissions caused by economic development and urban expansion(Feng et al., 2025; Y. Liu et al., 2023; Xie et al., 2016), synoptic meteorological patterns that bring high temperature, intense solar radiation, low humidity, low wind speed, and other unfavorable meteorological conditions, also play an important role in the formation and accumulation of ozone in various regions (Liu et al., 2024; Liu et al., 2025).

As a mesoscale weather system that forms and develops over the western Pacific Ocean, Tropical cyclones (TCs)

40   significantly influences the generation, accumulation, transport, and removal of ozone in Southeastern China (SEC) (Qu et al., 2021; J. Wang et al., 2024). Statistical analyses indicate that ozone pollution episodes are more likely to occur and persist before TCs land and after TCs dissipate (Xi et al., 2025a; Xi et al., 2025b), when the central location of TC is about 500~4500 km from land (Chen et al., 2021; Hu et al., 2023), when the intensity of at least a strong tropical storm grade (Qu et al., 2021), or when the moving track follows an offshore-turning or northward type (Deng et al., 2019; Lam et al., 2018;

45   Ding et al., 2023). Numerical simulations have further explored the combined effects of TC and the western Pacific subtropical high (WPSH) (C. Liu et al., 2023; Ouyang et al., 2022; Shu et al., 2016), TC-induced stratospheric ozone intrusion (Chen et al., 2022; Zhan and Xie, 2022), changes in the vertical structure of the boundary layer and ozone concentration by TC (He et al., 2021; Huang et al., 2021; Li et al., 2022), enhancement of TC on biogenic emissions and cross-regional transport (Wang et al., 2022; N. Wang et al., 2024; Xu et al., 2023), and complex regional ozone variations

50   caused by consecutive TCs (J. Wang et al., 2024; Zhan et al., 2020). Moreover, through the Integrated Process Rate (IPR) method provided by atmospheric chemical models, previous studies have elucidated the impacts of TCs on tropospheric ozone in SEC via generation, transport, and other related processes (Ouyang et al., 2022; Qu et al., 2021; Xu et al., 2024). However, current quantitative studies of TCs impact on ozone primarily focus on physical and chemical process contributions. Complex interactions with other weather systems pose challenges in isolating and quantifying the specific

55   contribution of TC and its intensity variations (Ouyang et al., 2022; Hu et al., 2024).

To reduce vortex initial position and intensity errors on forecast accuracy in TC simulations, the vortex separation and construction theory along with subsequent improvements proposed by (Kurihara et al., 1993; Kurihara et al., 1995), are commonly used combined with TC relocation to reconstruct vortex structures (Xu et al., 2019; Huang et al., 2018; Wu et al., 2020). This method not only improves the accuracy of numerical weather prediction but also provides a foundation for

60   quantifying the contributions of TC and its intensity. For example, Tang et al. (2023) conducted sensitivity experiments that separated the effects of multiple tropical cyclones one by one to investigate the mechanism of the extremely heavy rainfall in Henan Province in 2021. Similarly, Zhao et al. (2021) systematically analyzed the effects of Typhoon Lekima (2019) on extreme heat days along the southeastern coast of China by comparing a control WRF simulation with sensitivity experiments that removed either the entire vortex or only its horizontal wind from the initial conditions. Furthermore, Lin et

65   al. (2024) utilized the bogus model and found that the existence of TC enhanced the regional easterly wind anomaly over the

North China Plain (NCP), thereby causing a positive anomaly in surface PM2.5 concentration. However, the application of vortex removal methods in quantifying TC contributions to ozone remains relatively limited.

The Northward TC, as an important weather pattern influencing the interannual fluctuations of autumn ozone concentrations in SEC (Hu et al., 2023; Hu et al., 2024), clarifying how its varying intensities regulate meteorological conditions and atmospheric circulation to differentially impact ozone concentration changes, can provide crucial scientific support for developing targeted ozone management strategies during periods of northward TC influence. Therefore, this study employs observational and reanalysis data to statistically analyze the effects of meteorological factors and atmospheric circulation patterns on SEC ozone under different intensities of northward TCs during autumn from 2014 to 2024. Furthermore, through WRF-CMAQ numerical simulation and TC intensity sensitivity experiments, we quantitatively evaluate the contributions of TC intensity and location to SEC ozone during two severe ozone pollution episodes.

2 Data and methods

2.1 Data

Hourly ozone concentration monitoring data in autumn from 2014 to 2024 were obtained from the China National Environmental Monitoring Centre (available at http://www.cnemc.cn/en/, last access: 19 November 2025). The maximum daily 8 h average (MDA8) ozone concentration is calculated based on the hourly concentration values.

The TC track information, including position and intensity at a temporal resolution of 6 h used in this study was obtained from the China Meteorological Administration (CMA) Tropical Cyclone Data Centre (available at https://tcdata.typhoon.org.cn/, last access: 19 November 2025; (Lu et al., 2021; Ying et al., 2014). The TC intensity is classified into six categories based on the maximum sustained wind speed near its surface centre: Tropical Depression (TD: 10.8-17.1 m s^{-1}), Tropical Storm (TS:17.2-24.4 m s^{-1}), Severe Tropical Storm (STS: 24.5-32.6 m s^{-1}), Typhoon (TY: 32.7-41.4 m s^{-1}), Severe Typhoon (STY: 41.5-50.9 m s^{-1}), and Super Typhoon (SSTY: ≥51.0 m s^{-1}).

The European Centre for Medium-Range Weather Forecasts (ECMWF) Reanalysis v5 (ERA5) dataset (available at https://cds.climate.copernicus.eu/, last access: 19 November 2025), with a horizontal resolution of 0.25° × 0.25° and a time interval of 6 h, was used to analyze the meteorological conditions and atmospheric circulation patterns during different intensity periods of TC. The parameters extracted include 2 m temperature (T$_2$), surface solar radiation downwards (SSRD), boundary layer height (PBLH), 850 hPa and 10 m zonal and meridional wind speed, 850 hPa Vertical velocity, 1000 hPa relative humidity (1000 hPa RH), total cloud cover (TCC), total precipitation (TP), and 500 hPa geopotential height.

The 6 h Final Global Forecast System Operational Analysis (FNL) data with a resolution of 0.25° × 0.25° from the National Centre for Environmental Prediction (NCEP) were used to provide initial and boundary conditions for the WRF simulation (available at https://rda.ucar.edu/datasets/ds083.2/, last access: 19 November 2025). Additionally, the variables used for TC intensity sensitivity experiments include temperature (T), geopotential height (H), horizontal winds (U and V),

and relative humidity (RH) for the three-dimensional fields, as well as surface pressure (ps), surface temperature (ts), sea level pressure (pse), and surface horizontal winds (U_{10} and V_{10}) for the two-dimensional fields.

2.2 Model configuration

100   The WRF (v3.9.1)-CMAQ (v4.7.1) model was used to simulate two TC-related severe ozone pollution episodes that occurred in SEC (TC Mitag with maximum intensity TY: from 28 September to 2 October 2019; TC Muifa with maximum intensity STY: from 8-14 September 2022), and the track as well as intensity of two TCs are shown in Fig. 1(a). The WRF model was set with two one-way nested domains with horizontal resolutions of 27 and 9 km (Fig. 1b). The outer domain (d01) covers most of East Asia with 283 × 184 grids, while the inner domain (d02) covers most parts of South China with

105   250 × 190 grids with the PRD and the central-northern part of Zhejiang Province (ZJ) are represented by orange and red boxes, respectively (Fig. 1b). The model applies the WRF Single-Moment 6-class scheme microphysics scheme, Rapid Radiative Transfer Model (RRTM) longwave scheme, Goddard shortwave scheme, revised MM5 Monin-Obukhov surface layer scheme, Noah land surface model, Yonsei University planetary boundary layer scheme, and Betts-Miller-Janjic cumulus parameterization. Notably, the WRF simulations in this study were conducted using a daily re-initialization strategy

110   follow by Dong et al. (2018): with integrating the model for 36 h starting at 1200 UTC each day, then the first 12 h of the integration were discarded as model spin-up and the remaining 24 h were stitched together for a complete simulation over the typhoon period.
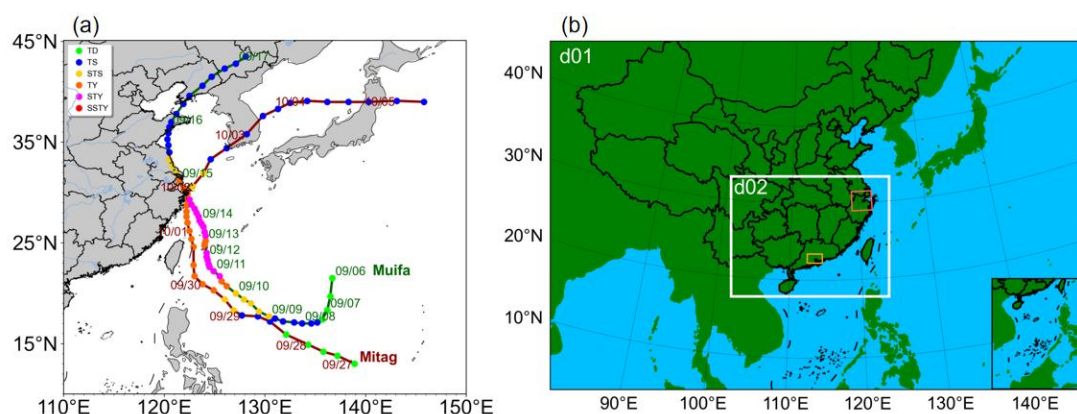
Figure 1: (a) The track and intensity of the TC Mitag (red text) and TC Muifa (green text). (b) The two nested model domains in the WRF-CMAQ model, along with the locations of the PRD (orange box) and ZJ (red box).

2.3 Sensitivity experiments design

In order to explore and quantify the contribution of TC to ozone, a series of experiments was conducted (Table 1). The control simulation (CTL) was performed using the settings described above to represent the original simulation results. Two sensitivity experiments were conducted to demonstrate the influence of TC on ozone in SEC. The first sensitivity experiment

120   (IT_TC) was identical to CTL except that the horizontal winds (U, V, U_{10}, and V_{10}) of the TC vortex were each doubled in

magnitude from the initial conditions. The second sensitivity experiment (NO_TC) removed the vortex of T, H, U, V, and RH for the three-dimensional fields, as well as ps, ts,pse, and surface horizontal winds (U_{10} and V_{10}) for the two-dimensional fields. Meanwhile, statistical analysis of the SSRD revealed that during periods of TC influence, the average solar radiation in SEC between 12:00 and 18:00 was 15.01 MJ m^{-2}, whereas during periods without northward TCs in autumn from 2014 to
125 2024 was only 9.41 MJ m^{-2} (not shown). This indicates that solar radiation in SEC is generally lower when there is no northward TC. Since the TC vortex removal method cannot directly modify cloud cover and solar radiation in the global field, we adjust the solar radiation and photolysis rate by a 37% reduction ((15.01 (MJ m^{-2}) - 9.41 (MJ m^{-2})) / 15.01 (MJ m^{-2}) * 100%) to more accurately simulate the radiation conditions during periods without northward typhoon in the NO_TC. The vortex filtering method proposed by (Kurihara et al., 1993; Kurihara et al., 1995) was adopted in this study, with other
130 meteorological variables adjusted through the dynamic and thermodynamic fields of the model itself to ensure better coordination between the filtering field and the model. Typhoon intensification follows a similar procedure, except that the horizontal winds are doubled and then re-interpolated into the environmental flow.

Table 1: Summary of numerical experiments performed in this study.

Experiment	Modifications
Control simulation (CTL)	Original numerical simulation.
Intensified TC (IT_TC)	Intensified TC vortex from the initial conditions, including the horizontal winds U, V, U_{10}, and V_{10}.
Removed TC along with reduced solar radiation and photolysis rate (NO_TC)	Removed TC vortex from the initial conditions (including T, H, U, V, and RH for the three-dimensional fields, as well as ps, ts, pse, U_{10}, and V_{10} for the two-dimensional fields), while simultaneously reducing both solar radiation and photolysis rate by 37%.

135   Taking 14:00 on 30 September 2019 as an example, the FNL analysis field was selected as the initial background field for the CTL to compare the sea-level pressure and 850 hPa wind fields of the NO_TC and the IT_TC. The results show that the CTL (Fig. 2a) exhibits a clear typhoon vortex to the east of Taiwan, whereas no or a very weak typhoon vortex is present after removing the typhoon (Fig. 2b). Comparing the 850 hPa wind fields of the CTL (Fig. 2c), the northward wind on the west side of the enhanced/removed typhoon strengthens/weakens (Figs. 2d and 2e), indicating that the vortex filtering
140 method can effectively enhance or remove the typhoon. Moreover, the difference between the vortex-filtered background field and the initial background field only exists within the typhoon vortex component, with no changes outside this region. That is to say, the background field after vortex filtering alters only the distribution of variables within the typhoon component, while the surrounding meteorological fields remain unchanged, which ensures the consistency of the large-scale

environmental field outside the typhoon component in the vortex-filtered background field. The vortex circulation after
145 filtering maintains good coordination and continuity with the surrounding large-scale environmental field, confirming that
this filtering method is both reasonable and feasible.
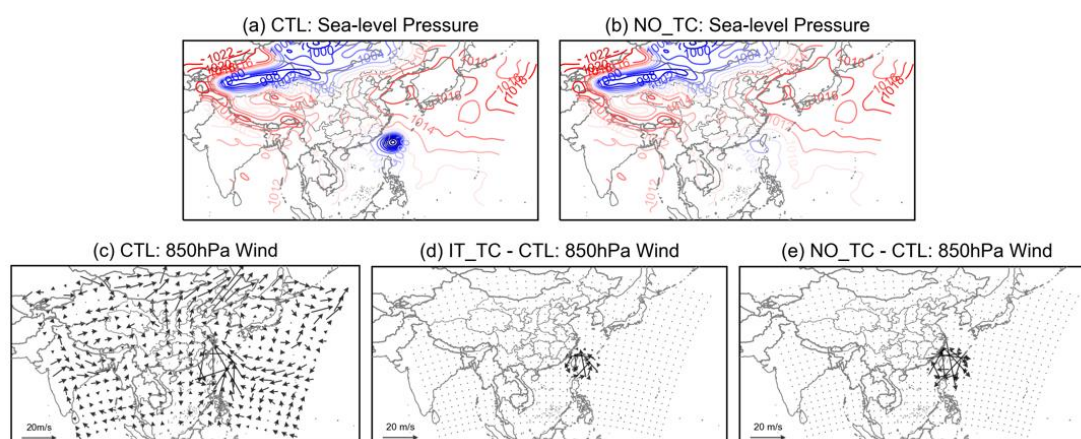
**Figure 2: Meteorological fields at 14:00 on 30 September 2019. Sea level pressure field for the CTL (a) and the NO_TC (b).
Differences with the CTL (c) in the IT_TC (d) and the NO_TC (e) of the 850 hPa wind field.**

3 Results and discussion

3.1 Relationship between TC intensity and ozone in SEC

3.1.1 Characteristics of ozone concentration

Figure 3a shows the time series of autumn MDA8 ozone concentration over the SEC from 2014 to 2024 (All Days
Mean, red line), with the blue and black dashed lines representing the average for days with TC (TC Days Mean) and
155 without TC (Non-TC Days Mean), respectively. The interannual variation of the mean MDA8 ozone concentration reveals a
fluctuating but overall increasing trend, with peak values occurring in 2019 and 2022. Throughout this period, ozone levels
on TC Days Mean consistently exceeded those on All Days Mean, particularly in 2022 when the difference reached 8 ppb. In
contrast, Non-TC Days Mean exhibited relatively lower ozone concentration without a significant linear trend over the 11
years period. These results demonstrate that TC activity has a significant influence on autumn ozone concentration in SEC.

160 Based on the analysis of Figure 3(a), the TC tracks over the northwest Pacific (west of 140°E) during autumn from
2014 to 2024 were classified into three distinct types: westward TCs (b), landfalling TCs (c), and northward TCs (d). The dot
sizes and colors represent the intensity of TCs and the MDA8 ozone levels in SEC corresponding to the positions of TCs,
respectively. Results show that westward TCs strengthen as they approach the southern side of the SEC, accompanied by
varying degrees of ozone concentration enhancement. When these TCs make landfall between 18-18.8°N subsequently, the
165 ozone concentration in SEC remains at a relatively high level. However, landfall over Hainan (southern area of SEC) induces
rapid ozone depletion across the entire SEC due to strong winds and precipitation (Fig. 3b). For landfalling TCs, both

intensity and ozone concentration in SEC initially increase then decrease during their approach, though overall ozone levels remain relatively low among the three TC types (Fig. 3c). During the period of the northward TC influence (Fig. 3d), ozone concentrations in SEC frequently exceeded 50 ppb, significantly higher than that of the other TC types. Notably, even TCs

170 located east of 135°E can drive substantial ozone increases when sufficiently intense. These findings demonstrate that TC intensity also plays an important role in influencing the ozone concentration of SEC, in addition to track type and location.
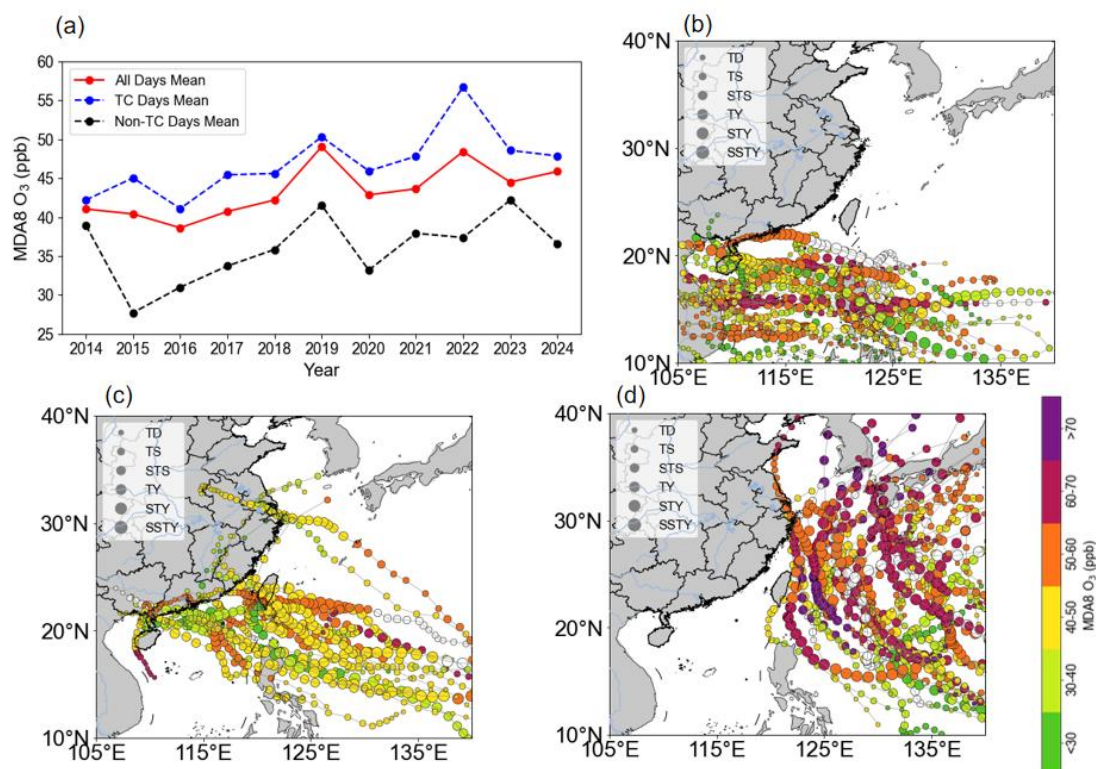
Figure 3: Time series of autumn average (red line), days with TC (blue dashed line), and days without TC (black dashed line) MDA8 ozone concentration over the SEC from 2014 to 2024. Tracks of westward TCs (b), landfalling TCs (c), and northward TCs
175 **(d), dot sizes represent TC intensities, and dot colors show the ozone concentration levels in SEC corresponding to the positions of TCs.**

To further investigate the influence of TC intensity on ozone in SEC, Figure 4 presents the ozone concentration across different TC intensity categories for each TC type. For westward TCs (Fig. 4a), both mean and median ozone concentration are obviously higher when TCs reach STY or SSTY intensity, suggesting that approaching but not yet landfalling TCs are
180 more conducive to ozone formation and accumulation in SEC. Landfalling TCs (Fig. 4b) show no clear ozone concentration trend with increasing intensity, with the mean ozone concentration at STY being even lower than that at TY. This may be attributed to enhanced ozone scavenging through intensified landfalling TCs circulation or peripheral convection (Lee et al., 2023; Ruan and Wu, 2018). In contrast, northward TCs (Fig. 4c) maintain higher ozone concentration than the other two types. Particularly when TCs reach TY or higher intensity, the mean, median, and 85th percentile of ozone concentration all

reach their highest levels. The findings above collectively identify intense northward TCs as a key contributor to elevated autumn ozone levels in SEC. Therefore, we will focus on the impact of northward TCs intensity on ozone in the SEC in the following sections.
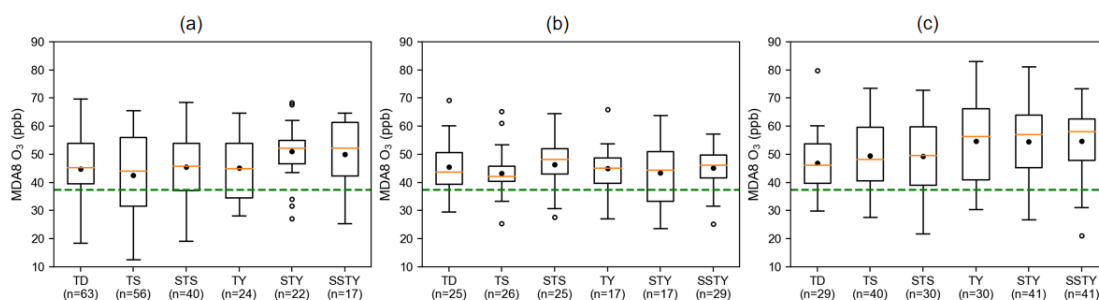
Figure 4: Ozone concentration corresponding to different intensities under westward (a), landfalling (b), and northward (c) TCs. The numbers on the x-axis represent the total number of days for that intensity, and the green dashed line indicates the average ozone concentration on days without TCs.

3.1.2 Meteorological conditions and atmospheric circulation characteristics

The differences in meteorological variables under varying intensities of northward TCs are compared in Figure 5 to explore their impacts on ozone concentration in SEC. Changes in ozone concentration are directly influenced by photochemical production rate, which primarily depends on solar radiation and temperature. As shown in Figs. 5(a) and (b), both T_2 and SSRD exhibit an overall increasing trend, indicating that the atmospheric photolysis conditions in SEC gradually intensify with the strengthening of TC intensity, thereby providing sufficient thermal driving force for the photochemical production of ozone. When TCs intensity reach TY, SSRD further strengthens (from 1.4 to 1.52 MJ m^{-2}), and the photochemical production rate of ozone reaches a stage peak, resulting in a significant increase in ozone concentration. It is noteworthy that in the subsequent STY and SSTY, T_2 and SSRD continue to intensify, yet ozone concentration does not increase significantly, indicating that photochemical production no longer dominates at this time.

In terms of dynamic effects, PBLH also shows a variation trend highly consistent with ozone concentration, indicating that a higher boundary layer height can effectively mix ozone and promote photochemical reactions of ozone precursors by expanding the reaction space (Tang et al., 2021; Zhang et al., 2023). Similarly, PBLH increases significantly during TY (from 726.03 to 825.89 m) and maintains high values subsequently (782.72 and 822.83 m). Meanwhile, WS$_{10}$ also increases obviously (from 3.74 to 4.26 m s^{-1}), and 850 hPa vertical velocity stabilizes at weak updrafts of approximately -0.01 Pa s^{-1} after STS. This suggests that the peripheral circulation of TCs may entrain precursors and ozone from upstream regions into the higher boundary layer through enhanced horizontal transport, and the superposition of weak vertical mixing and local photochemical production collectively leads to ozone accumulation.

On the other hand, wet scavenging processes also affect changes in ozone concentration. From TD to TY, especially from TS to TY, 1000 hPa RH, TCC, and TP show an obvious decreasing trend, forming a favorable condition characterized by low humidity, few cloud cover, and weak precipitation that synergistically promotes ozone accumulation, resulting in

peak ozone concentration during TY. However, they all rebound during STY and SSTY, leading to enhanced wet scavenging effects (Lee et al., 2023; Ruan and Wu, 2018). At this time, although the conditions for photochemical production and

215 dynamic accumulation remain favorable, the enhanced wet scavenging process consumes more ozone than its production and accumulation, thereby limiting further increases in ozone.
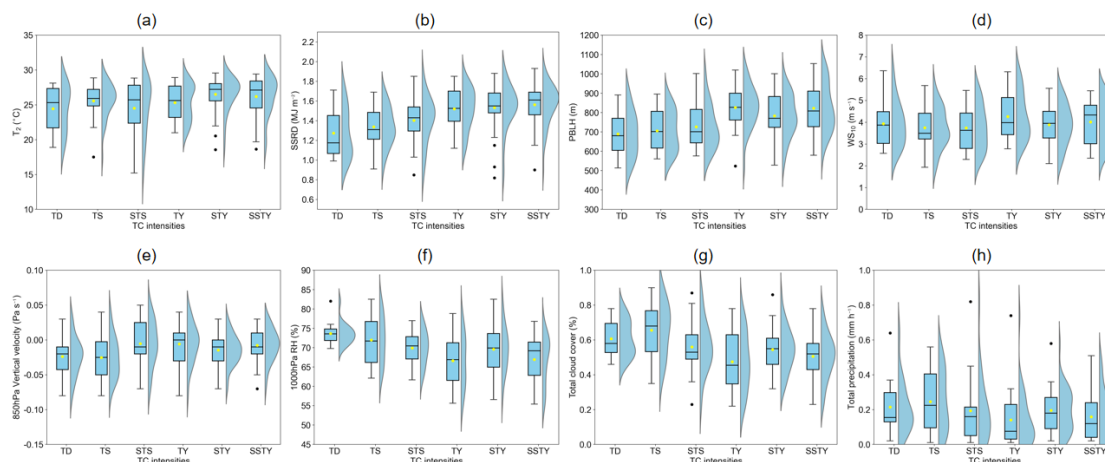
Figure 5: Comparison of meteorological conditions between different intensities of northward TCs. The box plot on the left shows basic statistical information about the data, while the violin plot on the right shows the distribution of the data.

220 Figure 6 illustrates the atmospheric circulation anomaly under different intensities of northward TCs relative to the autumn climatology (from 2014 to 2024). During TD to STS, positive geopotential height anomalies dominate north of 25°N, with weak cyclonic anomalies located east of the SEC. SEC is less affected by the northerly winds from the periphery of TCs, and the 1000 hPa RH along the coast of SEC exhibits positive anomalies at these periods (Figs. 6a–c). As TCs intensify to TY, anomalous high pressure shifts southward, exposing SEC to stronger TC-induced northerly flows (Fig. 6d). Notably,

225 while negative RH anomalies prevail throughout SEC during TY, their spatial extent diminishes at STY and SSTY, indicating enhanced anomalous cyclonic circulation influence from the east that elevates moisture (Figs. 6e–f).
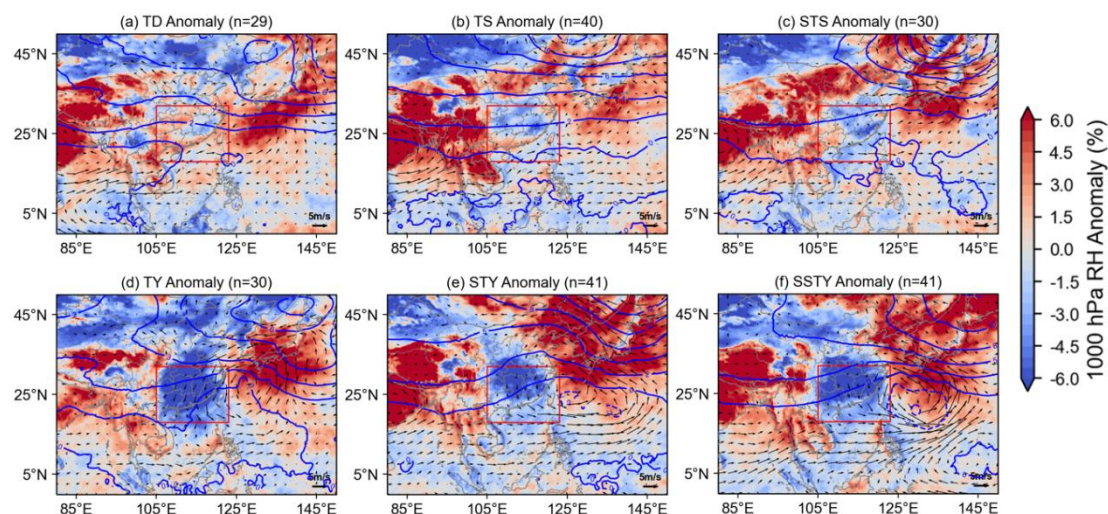
Figure 6: Composited anomalies of 500 hPa geopotential height (blue line), 850 hPa wind field (wind arrow), and 1000 hPa RH (color shade) under different intensities of northward TCs relative to the autumn climatology.

230   The above results suggest that steady ozone increases from TD to STS primarily result from photochemically driven production under enhanced solar radiation and elevated temperature, coupled with a rising boundary layer height that promotes ozone mixing and provides reaction space. When TCs intensity reach TY, photochemical activity, boundary layer height, vertical mixing, and horizontal transport are all at a favorable level, collectively leading to peak ozone concentration. Although meteorological conditions such as high temperature, strong solar radiation, elevated boundary layer height, and

235 low humidity remain generally favorable for ozone production during STY–SSTY, the enhanced wet scavenging begins to outweigh, and ozone concentration does not increase further.

3.2 Influence of TC intensity and position on ozone

   As analyzed in Section 3.1, when northward TCs intensify to TY, the ozone concentration in SEC reaches its maximum. Despite the continuous strengthening of TC intensity, the ozone concentration remains at a high level without further

240 increase. Based on the two years with the highest ozone concentration (2019 and 2022) in Figure 3(a), we select two severe ozone pollution episodes under the influence of northward TC with similar tracks to further explore the impact of TC intensity and location on ozone concentration in SEC.

3.2.1 Overview of two ozone episodes

   Figures 7a to 7j present the TC moving tracks, the daily 14:00 LT position of the WPSH (grey shading), and the

245 observed MDA8 ozone concentration across eastern China during two severe ozone pollution episodes (from 28 September to 2 October 2019 and from 8-15 September 2022). Before 28 September 2019 (Fig. 7a) and 8 September 2022 (Fig. 7f), persistent WPSH influence over southern China (not shown), which caused a downdraft that suppressed the vertical

dispersion of surface air pollutants. Enhanced solar radiation under the clear sky promoted efficient reactions of accumulated ozone precursors, resulting in widespread high ozone levels across eastern China. As the TCs developed and intensified

250   rapidly over the western Pacific, they crossed the ridge of high pressure all the way northward to the southeast of Taiwan, resulting in a break in the subtropical system (Figs. 7b and 7g). During the subsequent northward movement of TCs, SEC (except Fujian Province near the TCs centre) maintained high ozone levels (Figs. 7c and 7h). When the TCs made landfall along the coast of ZJ on 1 October 2019 (Fig. 7d) and 14 September 2022 (Fig. 7i), precipitation and strong winds significantly reduced ozone concentrations in this area. Although the overall ozone levels in SEC decreased (particularly in

255   ZJ) as the TCs generally moved away, PRD sustained high values (Figs. 7e and 7j).

Figures 7k and 7l further present the observed ozone time series for the entire d02 region (red line), the PRD (blue line), and the ZJ (black line) during two ozone pollution episodes. For the entire SEC, the afternoon ozone concentration approached or exceeded 75 ppb in the early period (before 30 September 2019 and before 13 September 2022), and then decreased significantly. The PRD region experienced afternoon ozone concentration exceeding 75 ppb throughout the TC

260   period. Notably, ozone concentration in ZJ showed a trend of being relatively high in the early period and decreasing significantly later (1-2 October 2019 and 13-14 September 2022).
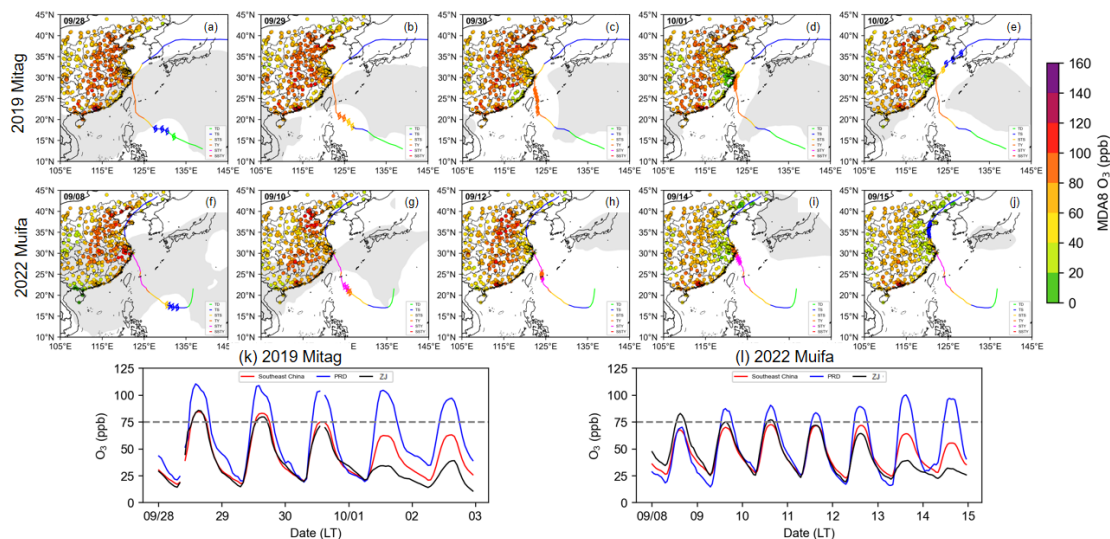
Figure 7: The TC moving track (line, with colors representing different intensities), the daily 14:00 LT position of the WPSH (gray shading), and the observed MDA8 ozone concentration across eastern China during two episodes (a-j). Diurnal variation in

265   **observed ozone concentrations for SEC (d02 domain, red line), PRD (blue line), and ZJ (black line) from 28 September to 2 October 2019 (k) and from 8-15 September 2022 (l).**

3.2.2 Control and intensification/removal sensitivity simulations of TCs

The WRF - CMAQ model was utilized to simulate the two TC-related ozone pollution episodes, and the ozone in the d02 domain was evaluated (Figure 8). It can be seen that the model captures the diurnal variation of ozone concentration in

270   two episodes, reproducing the characteristic pattern of a peak in the afternoon followed by a gradual decline at nighttime.

While slightly underestimating daytime maxima, the simulations achieved good performance metrics with correlation coefficients (R) and index of agreement (IOA) as high as 0.95, normalized mean biases (NMB) of -0.33% and -13.89%, and root mean square errors (RMSE) of 7.46 and 7.79 ppb. These results demonstrate that the model performance is within an acceptable range, giving confidence for conducting further analyses.
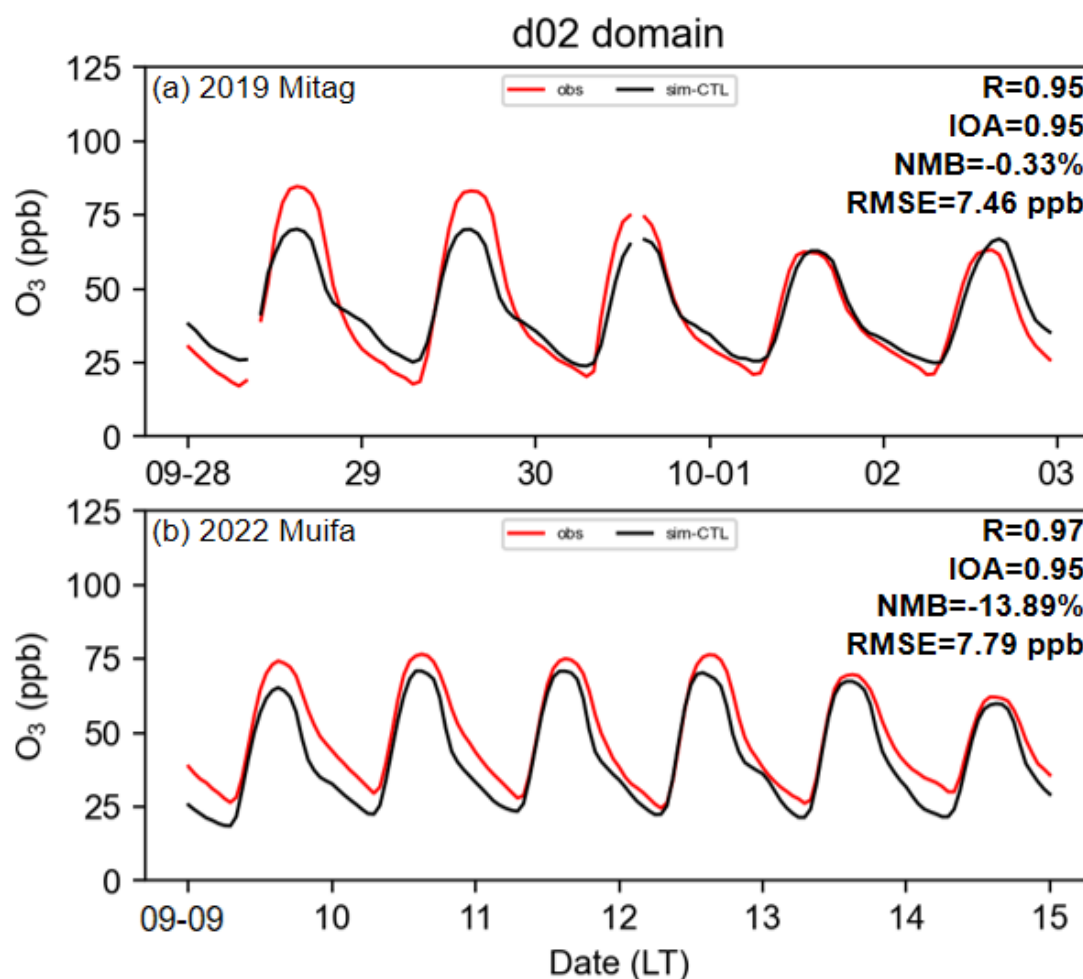
Figure 8: Hourly variations and statistical metrics of ozone in observed values (red line) compared to model simulations (black line) for SEC (d02 domain) from two ozone episodes.

Section 3.2.1 reveals that the two ozone pollution episodes shared similar TC moving tracks and consequently exerted comparable impacts on the ozone variations in SEC. Here, we selected three paired dates with similar TC locations in two episodes: 29 September 2019 and 10 September 2022, 30 September 2019 and 12 September 2022, as well as 1 October 2019 and 14 September 2022. Then categorized them into three periods according to the latitude where TC was located (20°N, 25°N, and 30°N) to further explore the impact of TC position on ozone concentration in different regions of the SEC.

Fig. 9 displays the spatial distribution of near-surface ozone and 10 m wind fields at 14:00 for the CTL. Ozone concentration in SEC along the peripheral northerly airflow region of TC remained at a relatively high level, particularly in PRD and
285 offshore areas. As TC moved northward and made landfall, ozone levels in ZJ decreased from about 100 ppb during the 20°N (Figure 9a) and 25°N (Figure 9b) periods to about 40 ppb at 30°N (Figure 9c).
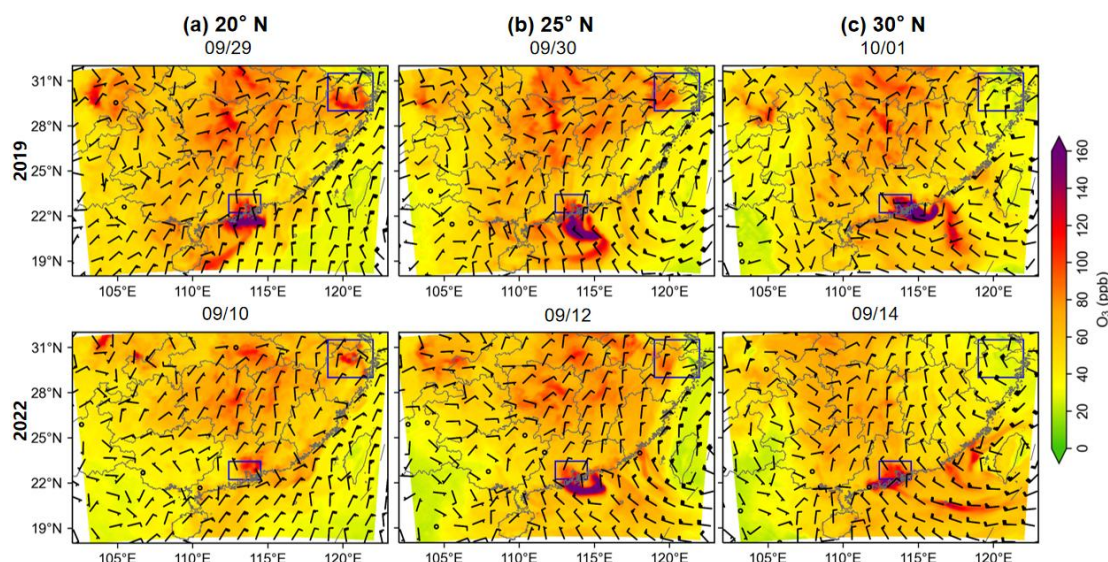
Figure 9: Spatial distribution of ozone and wind fields at ground level at 14:00 when TC was located at latitudes of (a) 20°N, (b) 25°N, and (c) 30°N during two episodes.

290 To investigate how various intensities of TC at different positions influence ozone over SEC, we conducted a comparative analysis of ozone differences between IT_TC (Figure 10) and NO_TC (Figure 11) sensitivity experiments. The IT_TC (Fig. 10) reveals an intensification of the northern wind at the centre and periphery of TC compared to the CTL, and most areas of the SEC exhibited relatively weak positive anomalies in ozone. That is to say, the TC enhancement did not lead to a significant increase in ozone concentration of SEC. In addition, the strong northerly wind also transported the
295 locally high-concentration ozone southward, reducing ozone levels in upstream areas such as the vicinity of ZJ and some parts of the PRD, while increasing ozone concentration in downwind areas like offshore PRD areas (Figs. 10a and 10b). On the other hand, as mentioned in Section 3.1, wet deposition process begins to dominate when TC intensity exceeds TY level. Consequently, for the TC Muifa in 2022 with a maximum intensity of STY, ozone concentration in coastal cities along SEC decreased by more than 10 ppb under its stronger influence on 12 September (bottom panel in Fig. 10b). After the enhanced
300 typhoon made landfall (Fig. 10c), precipitation and strong winds decreased ozone concentration by more than 10 ppb across western SEC compared to the CTL, with a greater range of decline during the 2022 Muifa TC period (bottom panel in Fig. 10c).
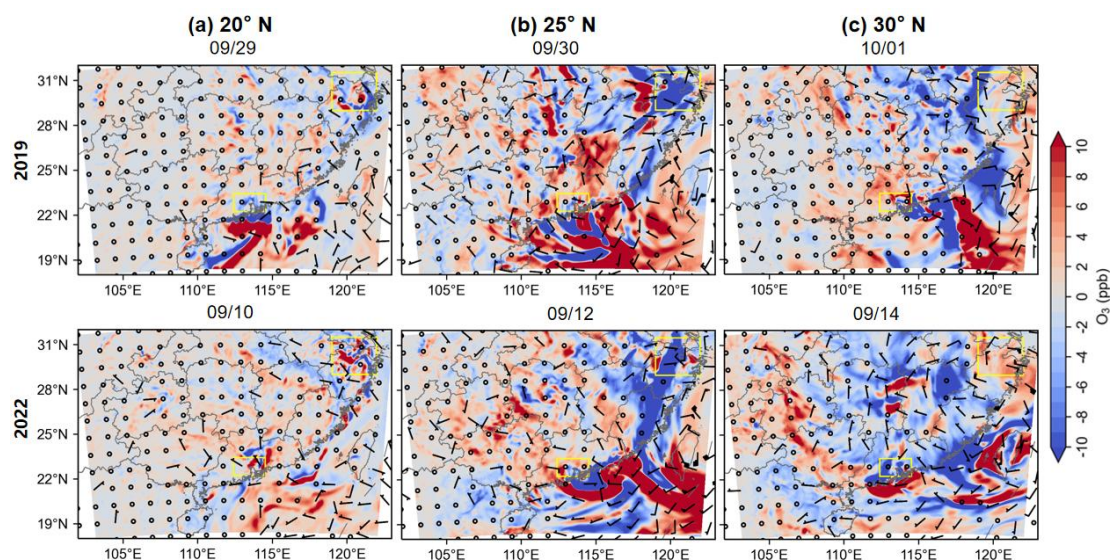
Figure 10: Difference with CTL of surface ozone and 10m wind fields in IT_TC.

305   After removing the influence of TC, the northerly wind weakened and the southward wind component enhanced (Fig. 11). More warm and moist air from the ocean increased the relative humidity, which, combined with weak solar radiation, collectively led to a reduction in ozone concentration of more than 10 ppb across most regions of the SEC. This indicates that, without the impact of the northward TC, the situation of high ozone concentration in most parts of the SEC would be alleviated. Notably, without the precipitation and strong winds brought by the TC landfall, ozone concentration in ZJ and its
310   surrounding areas on the east side of the SEC increased by more than 10 ppb (Figs. 11b and 11c).
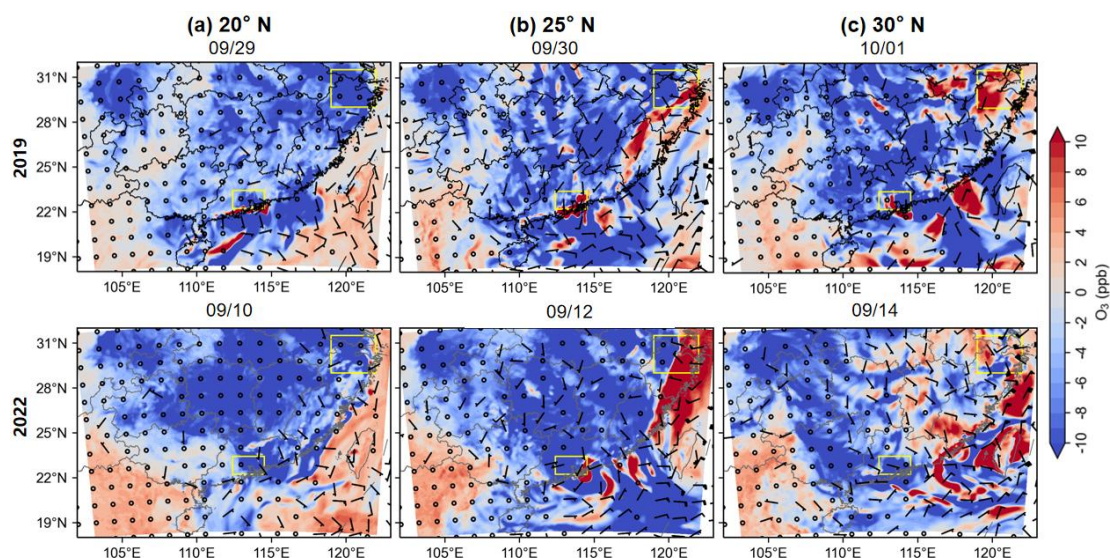
Figure 11: Same as Fig. 10 but for the NO_TC experiment.

Further insights can be seen from Figure 12, which compares atmospheric circulation and ozone vertical distribution during two ozone pollution episodes when TCs are in similar positions. During TC intensification (panels in the third row),
315   stronger northerly winds transport more ozone within the boundary layer from ZJ (A) to PRD (B). Consequently, ozone concentration along the line AB, particularly over PRD and the offshore sea area, increased compared to the CTL (Figs. 12a and d, b and e). As the intensified TC moved to 25°N, ozone concentration over ZJ began to decline significantly (Figs. 12b and 12e). This reduction became more pronounced upon TC landfall near 30°N (Figs. 12c and 12f), where stronger winds and precipitation effectively mitigated the high ozone across a broader region of ZJ. In NO_TC (panels in the fourth row),
320   reduced solar radiation weakened photochemical ozone production, leading to a general decrease in ozone within the boundary layer. Meanwhile, the reduction in wind speeds weakens horizontal transport at all levels along the line AB, causing ozone to accumulate over PRD rather than being blown outside the sea. Subsequently, due to the lack of wind and rainfall brought by the TC landfall, ozone concentration over ZJ increased relative to the CTL experiment (Figs. 12c and f).
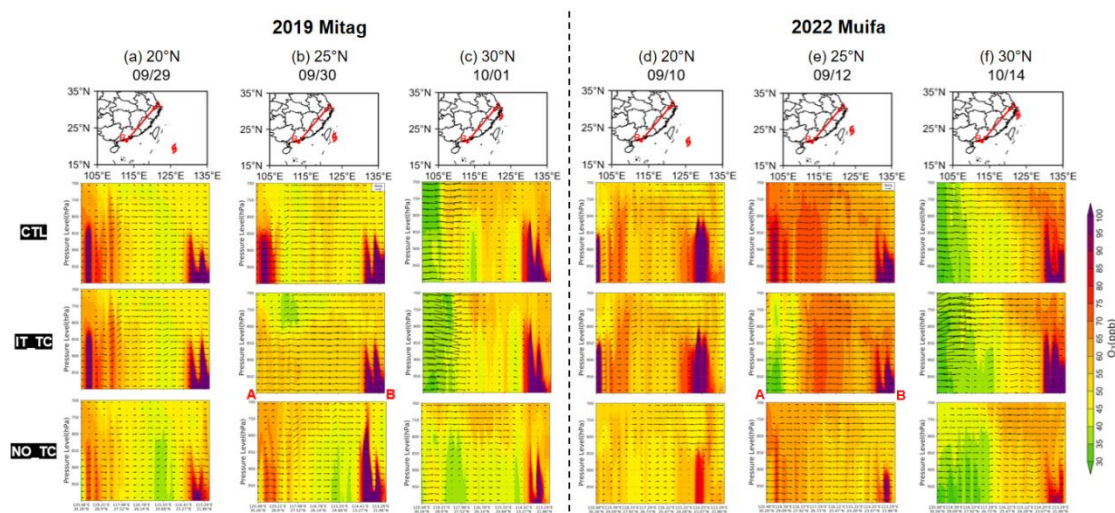
325   **Figure 12: Vertical distribution of ozone concentration (contours) and atmospheric circulation (wind vectors) over SEC (along the cross-section marked by the red line in the top-row panels) at 14:00 on the days with similar TC positions during the two episodes.**

In summary, an intensified TC initially enhances northerly winds over the SEC, leading to a slight increase in ozone concentration with downwind transport. Subsequently, as the TC makes landfall, improved diffusion conditions and precipitation lead to a more pronounced ozone reduction in ZJ and surrounding areas. Conversely, when there is no TC,
330   strengthened southerly winds bring more warm and humid marine air, coupled with reduced solar radiation, which causes the ozone concentration in the boundary layer of the SEC to decline by more than 10 ppb overall. Later, the lack of TC-induced rainfall and strong winds contributes to elevated ozone concentrations in the ZJ region.

3.2.3 Changes in BVOCs caused by solar radiation alterations

On the other hand, the high temperature and intense solar radiation associated with the TC periphery can induce more
335 biogenic VOC (BVOCs) emissions from forest areas in southern China(Wang et al., 2022; Kou et al., 2023), which are
important precursors to ozone formation. Since isoprene (ISOP) is the most abundant BVOC species in the forest areas of
southern China (Zheng et al., 2010; Li et al., 2023; N. Wang et al., 2024), we employ ISOP as a representative indicator of
BVOC emissions to investigate the impact of solar radiation differences on BVOCs emissions between conditions with and
without TC. Figures. 13a and 13b present the variability rate of ISOP caused by solar radiation changes before and after
340 removing TC during two ozone pollution episodes, showing that when solar radiation changes by 37%, the ISOP
concentration in SEC exhibits a corresponding linear reduction of 37%. This led to an overall decline of approximately 1 ppb
in ozone concentration (averaged from 12:00 to 18:00 during the ozone pollution episodes), with a drop of about 3 ppb in the
PRD and the central part of SEC, followed by the ZJ of around 2 ppb (Figs. 13c and 13d). In other words, changes in
BVOCs emissions due to altered solar radiation contributed approximately 1-3 ppb to the ozone production. This range of
345 BVOCs emissions contribution is lower than Wang et al. (2022) in PRD between 2014–2018 (from an average of 16.9% in
summer to 26.6% during TC periods) or Xu et al. (2023) in Beijing-Tianjin-Hebei during TC In-Fa (2021, 10 ppb), which
may be related to differences in the research season or the types of TC selected.
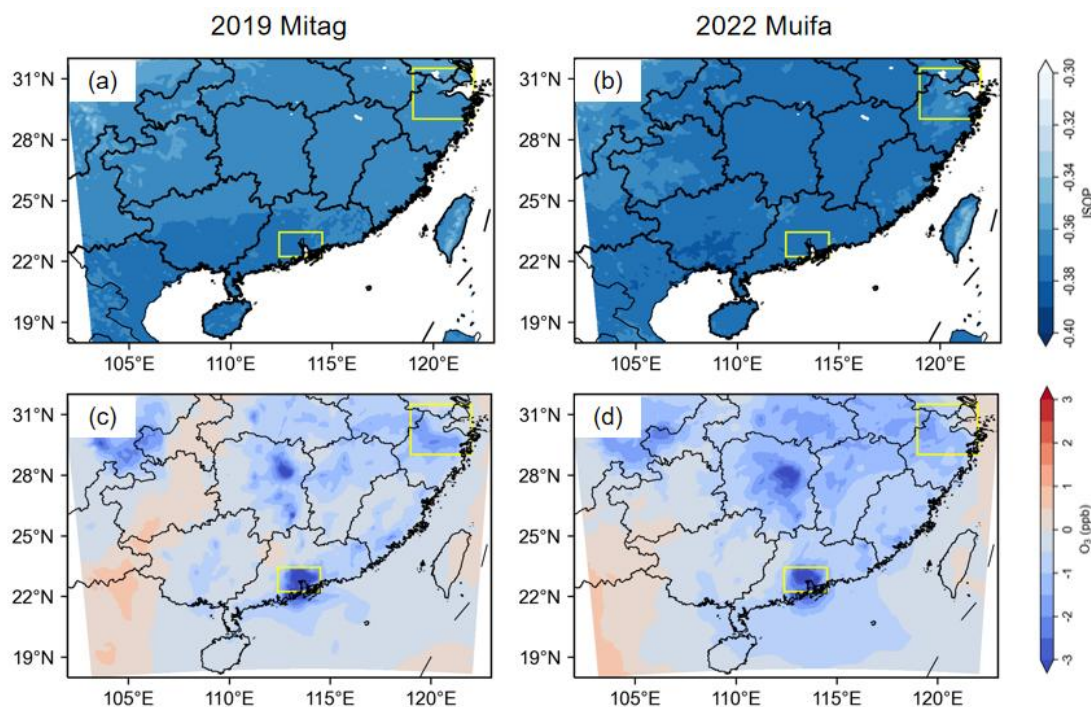
Figure 13: Variability rate of ISOP caused by radiation changes during two ozone pollution episodes (a and b). Changes in ozone
350 **concentration due to reduced BVOCs emissions resulting from decreased solar radiation (c and d).**

3.2.4 Regional ozone budgets in different experiments

To further elucidate the contribution of TCs with varying intensities (different TC experiments) to ozone inside the boundary layer in different SEC regions (PRD and ZJ) at distinct latitudinal positions (TC movement across latitudes), Table 3 summarizes the daytime (08:00-18:00) average contributions of individual processes results during two ozone pollution
355 episodes. When the TC was positioned at 20°N, photochemical production (CHEM) constituted the primary ozone source in both regions (2.13 ppb h^{-1} for PRD and 1.64 ppb h^{-1} for ZJ). Horizontal transport (HTRA) mainly showed negative contributions, and vertical transport (VTRA) exhibited regional variations. This indicates that even with prevailing northerly winds at the TC periphery driving southward ozone transport, photochemical processes remained dominant when TCs approached the SEC. Upon TC intensification (IT_TC), the contributions of individual processes to ozone in ZJ showed
360 minimal changes, suggesting limited influence of enhanced TCs at lower latitudes on the northern SEC. In PRD, the positive contribution of CHEM decreased slightly, while the negative contribution of HTRA weakened, demonstrating that intensified northerly winds generally enhanced ozone transport to southern SEC (PRD). For NO_TC, the reduced positive CHEM contribution and significantly weakened negative HTRA contribution further confirmed that both diminished solar radiation and decreased northerly winds transport collectively led to ozone reduction across the SEC.

365 When the TC moved to 25°N, the contributions of various processes exhibited regional divergence with changes in TC intensity. Compared to CTL, both regions in IT_TC showed reduced CHEM contribution, with ZJ experiencing a more pronounced decrease. The change in HTRA is similar to that when the TC is at 20°N. This indicates that although TC enhancement still facilitated outward horizontal transport, the increase in relative humidity (not shown) simultaneously suppressed photochemical production of ozone. In NO_TC, the lack of TC-induced uplifting compensation resulted in
370 stronger downdraft over ZJ (VTRA: 1.1 ppb h^{-1}), whereas PRD was dominated by localized updraft, yielding a more negative VTRA (-1.02 ppb h^{-1}).

As the TC made landfall at 30°N, PRD showed minimal variations in individual process contributions between CTL and IT_TC (CHEM: 1.9 and 1.94 ppb h^{-1}; HTRA: -0.23 and -0.22 ppb h^{-1}; VTRA: -1.38 and -1.49 ppb h^{-1}) due to weaker TC circulation influence. In contrast, ZJ exhibited significantly enhanced negative CHEM contribution in IT_TC resulting
375 from TC landfall-induced precipitation. Meanwhile, intensified convergence airflows caused HTRA in ZJ to shift from negative to positive (0.86 ppb h^{-1}). Under NO_TC, with the disappearance of TC-induced disturbances, the HTRA contribution in PRD transitioned from negative to positive, while CHEM in ZJ rebounded to -0.04 ppb h^{-1}.

Table 2: Daytime (08:00-18:00) mean contributions of individual processes for TCs with varying intensities to ozone within the boundary layer in different SEC regions at distinct latitudinal positions.

(ppb h^{-1})	CTL		IT_TC		NO_TC	
	20°N					
	PRD	ZJ	PRD	ZJ	PRD	ZJ
CHEM	2.13	1.64	1.87	1.66	1.69	0.82

	PRD	ZJ	PRD	ZJ	PRD	ZJ
HTRA	-1.35	-2.01	-1.11	-2.05	-0.25	-1.21
VTRA	-0.38	0.74	-0.33	0.74	-0.58	0.74
25°N						
	PRD	ZJ	PRD	ZJ	PRD	ZJ
CHEM	2.04	1.15	1.68	0.79	1.9	0.8
HTRA	-1.37	-2.35	-0.62	-1.96	-0.17	-1.84
VTRA	-0.36	0.34	-0.52	0.77	-1.02	1.1
30°N						
	PRD	ZJ	PRD	ZJ	PRD	ZJ
CHEM	1.9	-0.35	1.94	-0.51	1.44	-0.04
HTRA	-0.23	-0.15	-0.22	0.86	0.85	-0.25
VTRA	-1.38	0.42	-1.49	-0.33	-1.67	0.49

380

These results indicate that, when the TC is at 20°N, photochemical production dominates ozone formation, with TC enhancement primarily promoting southward transport of ozone. TC removal leads to concurrent radiation reduction and transport weakening, collectively decreasing regional ozone levels. As the TC moves to 25°N, while the enhanced TC favors horizontal transport, the accompanying RH increase suppresses the photochemical production of ozone. Without TC, strengthened downdraft occurs over ZJ, while ozone in the boundary layer of PRD diffuses outward to a greater extent. During TC landfall at 30°N, individual process contributions in PRD remain relatively stable as the TC intensifies, whereas ZJ shows intensified chemical consumption due to precipitation and strong winds. The photochemical production in ZJ roughly recovers when TC influences are removed.

4 Summary and conclusions

390   Autumn ozone pollution episodes in SEC are often associated with northward TCs in the Northwest Pacific Ocean. Based on observational and reanalysis data during autumn from 2014 to 2024, this study systematically examines the impacts of relevant meteorological variables and atmospheric circulation patterns associated with northward TCs of varying intensities on ozone in the SEC. Additionally, by carrying out the WRF-CMAQ model simulations with TC intensity sensitivity experiments, we quantitatively explore the contributions of TC intensity and position to ozone variations across different regions of the SEC during two severe ozone pollution episodes. Results show that the interannual variation of MDA8 ozone in autumn (2014-2024) over the SEC is consistent with TC activity, with relatively intense northward TCs playing a crucial role. Under the influence of these TCs, ozone concentration exhibits a steady increase when TC intensity evolves from TD to STS, which is mainly driven by enhanced photochemical production. As TC intensity reaches TY, photochemical activity, boundary layer height, horizontal transport, and vertical mixing all develop to favorable levels,

400   collectively leading to peak ozone concentration. Although favorable photochemical conditions such as high temperature and strong solar radiation persist from STY to SSTY and maintain high ozone levels, enhanced wet deposition triggered by TC-periphery convection suppresses further ozone accumulation.

By applying a vortex filtering method in the WRF numerical model to intensify or remove the meteorological variables related to the TC vortex during two severe ozone pollution episodes, we find that the intensification of TC enhanced
405   northerly winds over the SEC, causing a slight increase in ozone with southward transport. As TCs made landfall, improved diffusion conditions and precipitation led to more pronounced ozone reduction in ZJ and the surrounding areas. Conversely, TC removal weakened northerly wind transport, combined with reduced solar radiation, led to a widespread ozone decrease across the SEC by more than 10 ppb. Changes in BVOCs emissions due to altered solar radiation contributed approximately 1-3 ppb. Moreover, the results of the process analysis show that when the TC is at 20°N, photochemical production
410   dominates ozone formation, with TC enhancement promoting southward transport while TC removal reduces ozone concentration. As TC moved to 25°N, although an intensified TC facilitates horizontal transport, the increase in RH suppresses photochemical production of ozone. TC removal induces pronounced regional divergence in vertical transport. When TC makes landfall at 30°N, PRD remains relatively unaffected, whereas enhanced TCs accelerate ozone depletion in ZJ, a pattern that reverses with TC removal and photochemical production largely recovers.

415   Previous studies have investigated the relationship between TCs and ozone in the SEC, but most focused on qualitative comparisons of ozone levels with and without TC influence. In this study, we reveal the impact of northward TC intensity on ozone in the SEC and quantitatively evaluate the contribution of TCs using a vortex filtering method, which is crucial for deepening understanding of TC roles in ozone pollution and for optimizing emission control strategies. In the context of global warming, TCs are expected to become stronger (Wu et al., 2022; Xu et al., 2024) and more likely to move northward
420   (Cao et al., 2025; Nie et al., 2023), with extreme weather events projected to be frequent and intense. Therefore, the potential impacts of northward TCs and associated large-scale circulation on surface ozone in SEC merit further study. Notably, TC tracks and intensities are strongly modulated by non-linear interactions with large-scale circulation, particularly the WPSH (Pandey, 2025; Sun et al., 2015; Wu et al., 2020). After the removal of the TCs associated with the two severe ozone pollution episodes selected in this study, the SEC returned to the control of the WPSH (not shown). More accurate
425   quantification of TCs and WPSH impacts on ozone in the SEC and across eastern China can be achieved through further sensitivity experiments that simultaneously consider the WPSH influences.

Data availability

Hourly surface ozone was obtained from the China National Environmental Centre (http://www.cnemc.cn/en/, last access: 19 November 2025). The TC best track dataset was available from the China Meteorological Administration (CMA) Tropical
430   Cyclone Data Centre (available at https://tcdata.typhoon.org.cn/, last access: 19 November 2025). The ERA5 data were acquired from European Centre for Medium-Range Weather Forecasts Reanalysis v5 dataset

(https://cds.climate.copernicus.eu/, last access: 19 November 2025). The FNL meteorological data were taken from the National Centre for Environmental Prediction (https://rda.ucar.edu/, last access: 19 November 2025). Model output data of this paper are available upon request.

Author Contributions

TD and SL proposed the essential research idea. SO and JC performed the model simulations work and carried out the model output data analysis. SO wrote the original paper with input from TD, SL and RL. TD, SL, and RL helped revised the paper. JY, YH, and XC discussed the results and offered valuable comments.

Competing interests

The authors declare that they have no conflict of interest.

Acknowledgments

We would like to acknowledge the China National Environmental Centre, the European Centre for Medium-Range Weather Forecasts and the National Centre for Environmental Prediction for providing datasets that made this work possible. The numerical calculations were performed on the Guangdong Meteorological Service. We also acknowledge the support of the College of Environment and Climate, Institute for Environmental and Climate Research, Jinan University and the Guangdong Provincial Key Laboratory of Regional Numerical Weather Prediction, Guangzhou Institute of Tropical and Marine Meteorology of China Meteorological Administration, GBA Academy of Meteorological Research.

Financial support

This research was supported by the National Key Research and Development Program of China (grant number 2023YFC3709201, 2023YFC3706204), the National Natural Science Foundation of China (grant number 42275123, 42405194), Guangdong Provincial Science and Technology Collaborative Innovation Project for Social Development (grant number 2024A1111120022), the Guangdong Basic and Applied Basic Research Foundation (grant number 2023A1515012448, 2023A1515012205, 2024A1515510025), the Special Fund Project for Science and Technology Innovation Strategy of Guangdong Province (grant number 2019B121205004), the Key Innovation Team of Key Innovation Team of China Meteorological Administration (grant number CMA2023ZD08), the Science and Technology Research Project of Guangdong Meteorological Bureau (grant number GRMC2025M18).

References

Chen, Z., Liu, J., Cheng, X., Yang, M., and Wang, H.: Positive and negative influences of typhoons on tropospheric ozone over southern China, Atmospheric Chemistry and Physics, 21, 16911-16923, doi:10.5194/acp-21-16911-2021, 2021.

460 Chen, Z., Liu, J., Qie, X., Cheng, X., Shen, Y., Yang, M., Jiang, R., and Liu, X.: Transport of substantial stratospheric ozone to the surface by a dying typhoon and shallow convection, Atmospheric Chemistry and Physics, 22, 8221-8240, doi:10.5194/acp-22-8221-2022, 2022.

Cao, X., Wu, R., Jiang, X., Dai, Y., Wang, P., Lin, C., Deng, D., Sun, Y., Wu, L., Chen, S., Wang, Y., Xiao, X.: Future changes in tropical cyclone tracks over the western North Pacific under climate change, npj climate and atmospheric science,

465 8, 148, doi:10.1038/s41612-025-01036-6, 2025.

Deng, T., Wang, T., Wang, S., Zou, Y., Yin, C., Li, F., Liu, L., Wang, N., Song, L., Wu, C., and Wu, D.: Impact of typhoon periphery on high ozone and high aerosol pollution in the Pearl River Delta region, Science of the Total Environment, 668, 617-630, doi:10.1016/j.scitotenv.2019.02.450, 2019.

Ding, H., Kong, L., You, Y., Mao, J., Chen, W., Chen, D., Chang, M., and Wang, X.: Effects of tropical cyclones with

470 different tracks on ozone pollution over the Pearl River Delta region, Atmospheric Research, 286, doi:10.1016/j.atmosres.2023.106680, 2023.

Dong, W., Lin, Y., Wright, J. S., Xie, Y., Xu, F., Yang, K., Li, X., Tian, L., Zhao, X., and Cao, D.: Connections Between a Late Summer Snowstorm Over the Southwestern Tibetan Plateau and a Concurrent Indian Monsoon Low-Pressure System, Journal of Geophysical Research-Atmospheres, 123, 13676-13691, doi:10.1029/2018jd029710, 2018.

475 Feng, L., Ma, D., Xie, M., and Xi, M. J. R. S.: Review on the Application of Remote Sensing Data and Machine Learning to the Estimation of Anthropogenic Heat Emissions, Remote Sensing, 17, 200, doi:10.3390/rs17020200, 2025.

Grulke, N. E. and Heath, R. L.: Ozone effects on plants in natural ecosystems, Plant Biology, 22, 12-37, doi:10.1111/plb.12971, 2020.

He, G., Deng, T., Wu, D., Wu, C., Huang, X., Li, Z., Yin, C., Zou, Y., Song, L., Ouyang, S., Tao, L., and Zhang, X.:

480 Characteristics of boundary layer ozone and its effect on surface ozone concentration in Shenzhen, China: A case study, Science of the Total Environment, 791, doi:10.1016/j.scitotenv.2021.148044, 2021.

Hu, T., Lin, Y., Liu, R., Xu, Y., Ouyang, S., Wang, B., Zhang, Y., and Liu, S. C.: What caused large ozone variabilities in three megacity clusters in eastern China during 2015-2020?, Atmospheric Chemistry and Physics, 24, 1607-1626, doi:10.5194/acp-24-1607-2024, 2024.

485 Hu, W., Liu, R., Chen, Z., Ouyang, S., Hu, T., Wang, Y., Cui, Z., Jiang, B., Chen, D., and Liu, S. C.: Processes conducive to high ozone formation in Pearl River Delta in the presence of Pacific tropical cyclones, Atmospheric Environment, 307, doi:10.1016/j.atmosenv.2023.119859, 2023.

Huang, T., Yang, Y., O'Connor, E. J., Lolli, S., Haywood, J., Osborne, M., Cheng, J. C.-H., Guo, J., and Yim, S. H.-L.: Influence of a weak typhoon on the vertical distribution of air pollution in Hong Kong: A perspective from a Doppler

490   LiDAR network, Environmental Pollution, 276, doi:10.1016/j.envpol.2021.116534, 2021.

Huang, Y., Xue, J., Feng, Y., Chen, Z., Zhang, C., Li, M., and Li, J.: An initialization scheme using forecast vortexes and its application in simulation of typhoons Linfa and Chan-hom in 2015, Journal of Tropical Meteorology, 34, 598-609, doi:10.16032/j.issn.1004-4965.2018.05.003, 2018 (in Chinese).

Jacob, D. J. and Winner, D. A.: Effect of climate change on air quality, Atmospheric Environment, 43, 51-63,

495   doi:10.1016/j.atmosenv.2008.09.051, 2009.

Kou, W., Gao, Y., Zhang, S., Cai, W., Geng, G., Davis, S., Wang, H., Guo, X., Cheng, W., Zeng, X., Mingchen, M., Wang, H., Wang, Q., Yao, X., Gao, H., and Wu, L.: High downward surface solar radiation conducive to ozone pollution more frequent under global warming, Science Bulletin, 68, doi:10.1016/j.scib.2023.01.022, 2023.

Kurihara, Y., Bender, M. A., and Ross, R. J.: An Initialization Scheme of Hurricane Models by Vortex Specification,

500   Monthly Weather Review, 121, 2030-2045, doi:10.1175/1520-0493(1993)121<2030:AISOHM>2.0.CO;2, 1993.

Kurihara, Y., Bender, M. A., Tuleya, R. E., and Ross, R. J.: Improvements in the GFDL Hurricane Prediction System, Monthly Weather Review, 123, 2791-2801, doi:/10.1175/1520-0493(1995)123<2791:IITGHP>2.0.CO;2, 1995.

Lam, Y. F., Cheung, H. M., and Ying, C. C.: Impact of tropical cyclone track change on regional air quality, Science of the Total Environment, 610, 1347-1355, doi:10.1016/j.scitotenv.2017.08.100, 2018.

505   Lee, M., Min, S.-K., and Cha, D.-H.: Convection-permitting simulations reveal expanded rainfall extremes of tropical cyclones affecting South Korea due to anthropogenic warming, npj Climate and Atmospheric Science, 6, 176, doi:10.1038/s41612-023-00509-w, 2023.

Li, L., Cao, J., and Hao, Y.: Spatial and species-specific responses of biogenic volatile organic compound (BVOC) emissions to elevated ozone from 2014-2020 in China, Science of the Total Environment, 868,

510   doi:10.1016/j.scitotenv.2023.161636, 2023.

Li, Y., Zhao, X., Deng, X., and Gao, J.: The impact of peripheral circulation characteristics of typhoon on sustained ozone episodes over the Pearl River Delta region, China, Atmospheric Chemistry and Physics, 22, 3861-3873, doi:10.5194/acp-22-3861-2022, 2022.

Lin, H., Ding, K., Huang, X., Lou, S., Xue, L., Wang, Z., Ma, Y., and Ding, A.: Impacts of Northward Typhoons on Autumn

515   Haze Pollution Over North China Plain, Journal of Geophysical Research: Atmospheres, 129, e2023JD040465, doi:/10.1029/2023JD040465, 2024.

Liu, B., Li, Y., Wang, L., Zhang, L., Qiao, F., Nan, P., Ji, D., Hu, B., Xia, Z., and Lou, Z.: Evaluating the effects of meteorology and emission changes on ozone in different regions over China based on machine learning, Atmospheric Pollution Research, 102354, doi:10.1016/j.apr.2024.102354, 2024.

520   Liu, C., He, C., Wang, Y., He, G., Liu, N., Miao, S., Wang, H., Lu, X., and Fan, S.: Characteristics and mechanism of a persistent ozone pollution event in Pearl River Delta induced by typhoon and subtropical high, Atmospheric Environment, 310, 119964, doi:10.1016/j.atmosenv.2023.119964, 2023.

Liu, N., He, G., Wang, H., He, C., Wang, H., Liu, C., Wang, Y., Wang, H., Li, L., Lu, X., and Fan, S.: Rising frequency of ozone-favorable synoptic weather patterns contributes to 2015-2022 ozone increase in Guangzhou, Journal of Environmental
525   Sciences, 148, 502-514, doi:10.1016/j.jes.2023.09.024, 2025.

Liu, Y., Geng, G., Cheng, J., Liu, Y., Xiao, Q., Liu, L., Shi, Q., Tong, D., He, K., and Zhang, Q.: Drivers of Increasing Ozone during the Two Phases of Clean Air Actions in China 2013–2020, Environmental Science & Technology, 57, 24, 8954–8964, doi:10.1021/acs.est.3c00054, 2023.

Lu, X., Zhang, L., and Shen, L.: Meteorology and Climate Influences on Tropospheric Ozone: a Review of Natural Sources,
530   Chemistry, and Transport Patterns, Current Pollution Reports, 5, 238-260, doi:10.1007/s40726-019-00118-3, 2019.

Lu, X., Yu, H., Ying, M., Zhao, B., Zhang, S., Lin, L., Bai, L., and Wan, R.: Western North Pacific Tropical Cyclone Database Created by the China Meteorological Administration, Advances in Atmospheric Sciences, 38, 690-699, doi:10.1007/s00376-020-0211-7, 2021.

Nie, X., Tan, H., Cai, R. and Gao, X.: Projection of the tropical cyclones landing in China in the future based on regional
535   climate model, Climate Change Research, 19(1): 23-37, doi:10.12006/j.issn.1673-1719.2022.064, 2023 (in Chinese).

Ouyang, S., Deng, T., Liu, R., Chen, J., He, G., Leung, J. C.-H., Wang, N., and Liu, S. C.: Impact of a subtropical high and a typhoon on a severe ozone pollution episode in the Pearl River Delta, China, Atmospheric Chemistry and Physics, 22, 10751-10767, doi:10.5194/acp-22-10751-2022, 2022.

Pandey, R. S.: Role of Position of Pacific Subtropical High in Deciding Path of Tropical Storms, Atmosphere, 16, 322,
540   doi:10.3390/atmos16030322, 2025.

Professional Committee of Ozone Pollution Control of Chinese Society for Environmental Sciences: The Bluebook: Prevention and Control of Ozone Pollution in China (2023), Science Press, Beijing, China, ISBN 978-7-03-078184-0, 2024 (in Chinese).

Qu, K., Wang, X., Yan, Y., Shen, J., Xiao, T., Dong, H., Zeng, L., and Zhang, Y.: A comparative study to reveal the
545   influence of typhoons on the transport, production and accumulation of O3 in the Pearl River Delta, China, Atmospheric Chemistry and Physics, 21, 11593-11612, doi:10.5194/acp-21-11593-2021, 2021.

Ruan, Z. and Wu, Q.: Precipitation, Convective Clouds, and Their Connections With Tropical Cyclone Intensity and Intensity Change, Geophysical Research Letters, 45, 1098-1105, doi:10.1002/2017GL076611, 2018.

Shu, L., Xie, M., Wang, T., Gao, D., Chen, P., Han, Y., Li, S., Zhuang, B., and Li, M.: Integrated studies of a regional ozone
550   pollution synthetically affected by subtropical high and typhoon system in the Yangtze River Delta region, China, Atmospheric Chemistry and Physics, 16, 15801-15819, doi:10.5194/acp-16-15801-2016, 2016.

Sun, Y., Zhong, Z., Yi, L., Li, T., Chen, M., Wan, H., Wang, Y., and Zhong, K.: Dependence of the relationship between the tropical cyclone track and western Pacific subtropical high intensity on initial storm size: A numerical investigation, Journal of Geophysical Research: Atmospheres, 120, 11,451-411,467, doi:10.1002/2015JD023716, 2015.

555 Tang, G., Liu, Y., Huang, X., Wang, Y., Hu, B., Zhang, Y., Song, T., Li, X., Wu, S., Li, Q., Kang, Y., Zhu, Z., Wang, M., Wang, Y., Li, T., Li, X., and Wang, Y.: Aggravated ozone pollution in the strong free convection boundary layer, Science of The Total Environment, 788, 147740, doi:10.1016/j.scitotenv.2021.147740, 2021.

Tang, J., Xu, X., Zhang, S., Xu, H., and Cai, W.: Response of remote water vapor transport to large topographic effects and the multi-scale system during the "7.20 " rainstorm event in Henan Province, China, Frontiers in Earth Science, 11,
560 doi:10.3389/feart.2023.1106990, 2023.

Trainer, M., Parrish, D. D., Goldan, P. D., Roberts, J., and Fehsenfeld, F. C.: Review of observation-based analysis of the regional factors influencing ozone concentrations, Atmospheric Environment, 34, 2045-2061, doi:10.1016/S1352-2310(99)00459-8, 2000.

Wang, J., Wang, P., Tian, C., Gao, M., Cheng, T., and Mei, W.: Consecutive Northward Super Typhoons Induced Extreme
565 Ozone Pollution Events in Eastern China, Npj Climate and Atmospheric Science, 7, doi:10.1038/s41612-024-00786-z, 2024.

Wang, N., Huang, X., Xu, J., Wang, T., Tan, Z.-M., and Ding, A.: Typhoon-boosted biogenic emission aggravates cross-regional ozone pollution in China, Science Advances, 8, doi:10.1126/sciadv.abl6166, 2022.

Wang, N., Wang, H., Huang, X., Chen, X., Zou, Y., Deng, T., Li, T., Lyu, X., and Yang, F.: Extreme weather exacerbates ozone pollution in the Pearl River Delta, China: role of natural processes, Atmospheric Chemistry and Physics, 24, 1559-
570 1570, doi:10.5194/acp-24-1559-2024, 2024.

Wu, L., Zhao, H., Wang, C., Cao, J., Liang, J.: Understanding of the Effect of Climate Change on Tropical Cyclone Intensity: A Review. Advances in Atmospheric Sciences, 39, 205–221. doi:10.1007/s00376-021-1026-x, 2022.

Wu, Q., Wang, X. and Tao, L.: Interannual and interdecadal impact of Western North Pacific Subtropical High on tropical cyclone activity. Climate Dynamics, 54, 2237–2248, doi:10.1007/s00382-019-05110-7, 2020.

575 Wu, Z., Zhang, J., Chen, J., Pang, B., Xia, Y., and Chen, F.: The study on the method of conditional typhoon vortex relocation for GRAPES regional ensemble prediction, Acta Meteorologica Sinica, 78, 163-176, doi:10.11676/qxxb2020.027, 2020 (in Chinese).

Xi, M., Luo, Y., Li, Y., Ma, D., Feng, L., Zhang, S., Chen, S., and Xie, M.: Comprehensive analysis of prevailing weather patterns and high-impact typhoon tracks to reveal where and how tropical cyclone affects regional ozone pollution in the
580 Yangtze River Delta region, China, Atmospheric Environment, 361, 121498, doi:doi.org/10.1016/j.atmosenv.2025.121498, 2025a.

Xi, M., Xie, M., Gao, D., Ma, D., Luo, Y., Feng, L., Chen, S., and Zhang, S.: The impact of tropical cyclones on regional ozone pollution and its future trend in the Yangtze River Delta of China, Atmos. Chem. Phys., 25, 14573-14590, doi:10.5194/acp-25-14573-2025, 2025b.

585 Xie, M., Liao, J., Wang, T., Zhu, K., Zhuang, B., Han, Y., Li, M., and Li, S.: Modeling of the anthropogenic heat flux and its effect on regional meteorology and air quality over the Yangtze River Delta region, China, Atmos. Chem. Phys., 16, 6071-6089, doi:10.5194/acp-16-6071-2016, 2016.

Xu, D., Zhang, B., Zeng, Q., Feng, Y., Zhang, Y., and Dai, G.: A typhoon initialization scheme based on incremental analysis updates technology, Acta Meteorologica Sinica, 77, 1053-1061, doi:10.11676/qxxb2019.060, 2019 (in Chinese).

590 Xu, J., Zhang, Z., Zhao, X., and Zhang, J.: Synthetically impacts of the topography and typhoon periphery on the atmospheric boundary layer structure and special regional pollution pattern of O3 in North China Plain, Atmospheric Environment, 330, doi:10.1016/j.atmosenv.2024.120566, 2024.

Xu, J., Zhao, P., Chan, J. C. L., Shi, M., Yang, C., Zhao, S., Xu, Y., Chen, J., Du, L., Wu, J., Ye, J., Xing, R., Wang, H., and Lu, L.: Increasing tropical cyclone intensity in the western North Pacific partly driven by warming Tibetan Plateau, Nature
595 Communications, 15, 310, doi:10.1038/s41467-023-44403-8, 2024.

Xu, J., Zhou, D., Gao, J., Huang, X., Xue, L., Huo, J., Fu, Q., and Ding, A.: Biogenic emissions-related ozone enhancement in two major city clusters during a typical typhoon process, Applied Geochemistry, 152, doi:10.1016/j.apgeochem.2023.105634, 2023.

Ying, M., Zhang, W., Yu, H., Lu, X., Feng, J., Fan, Y., Zhu, Y., and Chen, D.: An Overview of the China Meteorological
600 Administration Tropical Cyclone Database, Journal of Atmospheric and Oceanic Technology, 31, 287-301, doi:10.1175/jtech-d-12-00119.1, 2014.

Zhan, C. and Xie, M.: Exploring the link between ozone pollution and stratospheric intrusion under the influence of tropical cyclone Ampil, Science of the Total Environment, 828, doi:10.1016/j.scitotenv.2022.154261, 2022.

Zhan, C., Xie, M., Huang, C., Liu, J., Wang, T., Xu, M., Ma, C., Yu, J., Jiao, Y., Li, M., Li, S., Zhuang, B., Zhao, M., and
605 Nie, D.: Ozone affected by a succession of four landfall typhoons in the Yangtze River Delta, China: major processes and health impacts, Atmospheric Chemistry and Physics, 20, 13781-13799, doi:10.5194/acp-20-13781-2020, 2020.

Zhan, Y., Xie, M., Zhao, W., Wang, T., Gao, D., Chen, P., Tian, J., Zhu, K., Li, S., Zhuang, B., Li, M., Luo, Y., and Zhao, R.: Quantifying the seasonal variations in and regional transport of PM2.5 in the Yangtze River Delta region, China: characteristics, sources, and health risks, Atmos. Chem. Phys., 23, 9837-9852, doi:10.5194/acp-23-9837-2023, 2023.

610 Zhang, C., Jiang, Z., Liu, M., Dong, Y., and Li, J.: Relationship between summer time near-surface ozone concentration and planetary boundary layer height in Beijing, Atmospheric Research, 293, 106892, doi:10.1016/j.atmosres.2023.106892, 2023.

Zhao, D., Lin, Y., Li, Y., and Gao, X.: An Extreme Heat Event Induced by Typhoon Lekima (2019) and Its Contributing Factors, Journal of Geophysical Research-Atmospheres, 126, doi:10.1029/2021jd034760, 2021.

Zheng, J., Zheng, Z., Yu, Y., and Zhong, L.: Temporal, spatial characteristics and uncertainty of biogenic VOC emissions in
615 the Pearl River Delta region, China, Atmospheric Environment, 44, 1960-1969, doi:10.1016/j.atmosenv.2010.03.001, 2010.